Article:

Faggetter, LE, Wignall, PB, Pruss, SB et al. (4 more authors) (2019) Mercury chemostratigraphy across the Cambrian Series 2 – Series 3 boundary: evidence for increased volcanic activity coincident with extinction? Chemical Geology, 510. pp. 188-199. ISSN 0009-2541

https://doi.org/10.1016/j.chemgeo.2019.02.006

Mercury chemostratigraphy across the Cambrian Series 2 – Series 3 boundary: evidence for increased volcanic activity coincident with extinction?

Faggetter, L.E., Wignall, P.B., Pruss, S.B., Jones, D.S., Grasby, S., Widdowson, M. Newton, R.J.

ABSTRACT

Flood basalt volcanism represented by the Kalkarindji Province (Australia) is temporally associated with a trilobite mass extinction at the Cambrian Series 2 – Series 3 boundary, providing one of the oldest potential links between volcanism and biotic crisis in the Phanerozoic. However, the relative timing of flood basalt volcanism (Kalkarindji Province, Australia) and the trilobite extinctions, first recorded in North America, is not known. Mercury (Hg) enrichment in the sedimentary record provides a potential proxy for volcanism which may facilitate improved chronologies of eruption and extinction. Here we report mercury records for three sections from mid-shelf strata of the Great Basin (western USA) that straddle the Series 2 – Series 3 boundary. One section (Oak Springs Summit, NV) features a Hg enrichment at the start of the extinction interval, but mercury anomalies are also present at lower levels. These older anomalies may record either earlier phases of Kalkarindji volcanism, eruptions in other locations, or may be the result of sedimentary and/or diagenetic processes affecting the Hg record. In the Carrara Formation at Emigrant Pass, CA, the precise extinction horizon is not well defined, but a carbon isotope anomaly (the Redlichiid-Olenellid Extinction Carbon isotope Event; ROECE) provides a stratigraphic tie point to the Oak Springs Summit section. At Emigrant Pass, Hg enrichments precede the ROECE interval and are absent in the inferred extinction zone. The Pioche Formation at Ruin Wash, NV, lacks Hg enrichment at the extinction horizon but contains older enrichments. The inconsistent Hg records between the three sections demonstrate that factors controlling Hg accumulation and preservation in marine sedimentary environments are not yet fully understood. The effects of redox fluctuations may complicate one-to-one association of sedimentary Hg enrichments and massive volcanism at the Cambrian Series 2 – Series 3 boundary and elsewhere in the geologic record.

1. INTRODUCTION

The temporal connection between large igneous province (LIP) eruptions and Phanerozoic mass extinction events is well established, and the associated cause and effect linkage compelling (e.g. Wignall, 2001, 2015; Courtillot and Renne, 2003; Kravchinsky, 2012; Ernst & Youbi, 2017). Biotic change and carbon isotope excursions are an established feature of the Cambrian, but their relationship to LIP volcanism is poorly understood. In this context, the favoured candidate Cambrian LIP is the Kalkarindji Province (including the Antrim lavas) of northern and western Australia; this has been dated by a single zircon (Milliwindi dyke) to yield a U-Pb age of 510.7 ± 0.6 Ma (Jourdan et al., 2014), demonstrating a close temporal relationship to the previously reported $^{40}Ar/^{39}Ar$ date of 507.5 ± 1.6 Ma determined for its extrusive portion (i.e. Antrim Lavas; Glass and Phillips, 2006). This LIP currently has a surface exposure of c. 425 000 km^2 in northern and central Australia (Veevers, 2001), but was likely erupted over a much larger area; its scattered remnants could indicate a possible original extent of >2 million km^2 (e.g. Glass and Phillips, 2006, Jourdan et al., 2014). Accordingly, the province may thus be dimensionally comparable with other significant Phanerozoic LIPs (e.g. Columbia River Basalts), especially since it may also correlate with volcanics of similar age and/or composition preserved in the Tarim Block in NW China and the North China Block (Li et al., 1996; 2008), and the Sibumasu terrane preserved in current day Thailand and Myanmar (Zhu et al., 2012; Cocks and Torsvik, 2013).

Dating of the Kalkarindji province indicates emplacement close to the Cambrian Series 2 – Series 3 boundary (traditionally Lower – Middle), and thus potentially contemporaneous with the extinction of the redlichiid and olenellid trilobites (Palmer, 1998; Jourdan et al., 2014; Zhang et al., 2015). The extinction of the olenellids has been well studied in detailed sections located in the western USA, but locating the horizon that coincides with the Kalkarindji eruptions has hitherto been difficult due to a lack of an eruption proxy within ancient marine sediments. Temporal correlation between the Kalkarindji LIP emplacement and the Series 2 – Series 3 boundary is based upon a U-Pb zircon date of 510.7 ± 0.6Ma (Jourdan et al., 2014), and the provisional age of the Series 2 – Series 3 boundary (~509 Ma, Ogg et al., 2016). The association of this LIP with trilobite extinction at the Series 2 – Series 3 boundary is therefore inferred on the basis of this temporal correlation (Glass and Phillips, 2006; Hough et al., 2006; Jourdan et al., 2014).

Testing a causal link between the Kalkarindji and the Series 2 – Series 3 trilobite extinction requires improved correlations between the volcanic event(s) and the trilobite extinction horizons. Recently, mercury (Hg) concentrations in the sedimentary record have provided a proxy for both regional and global volcanic activity (e.g. Schuster et al., 2002, albeit in ice-core, not sediments) and thus offers the potential to correlate the interval of extinction with evidence for volcanism in the same stratigraphic sections. The value of this technique has been demonstrated at several key mass extinction and oceanic anoxic events including those at the Ordovician–Silurian; latest Permian; Permian-Triassic; end-Triassic; early Jurassic and end-Cretaceous events (Sanei et al., 2012; Sial et al., 2013; 2014; Percival et al., 2015; Thibodeau et al., 2016; Font et al., 2016; Grasby et al., 2013; 2016; Bergquist, 2017; Gong et al., 2017; Jones et al., 2017; Percival et al., 2018). Here we present sedimentary Hg records for strata in which the trilobite extinction horizons have been constrained and evaluate the potential of the Kalkarindji LIP to produce this sedimentary geochemical record.

Volcanism represents a primary source of gaseous Hg^0 to Earth's surface; unlike other volcanic trace metals, its long atmospheric residence time (0.5-2 years) permits hemispheric circulation and establishes its potential as a tracer for volcanism (Pyle and Mather, 2003; Percival et al., 2015, 2017). Atmospheric oxidation of Hg^0 by halogens, ozone and radicals forms reactive Hg^{2+}, a soluble ion which is deposited during precipitation (wet deposition). Horowitz et al. (2017) found that, during its residence in the troposphere, Hg is most effectively oxidised by bromine (Br), forming atmospheric HgBr complexes. As the largest source of atmospheric Br is organobromines - which are produced as a by-product of phytoplankton photosynthesis - the most effective oxidation and wet deposition of Hg^{2+} occurs above and, subsequently to, the marine realm (Horowitz et al., 2017). In modern oceans ~49% of marine Hg deposition occurs in tropical oceans due to the greater availability of productivity-driven organobromines and other oxidising radicals at these latitudes (Horowitz et al., 2017). Once in the marine realm Hg^{2+} forms complexes with clay minerals (Kongchum et al., 2011), organic matter (Benoit et al., 2001), and, in anoxic/euxinic conditions, it can be scavenged from seawater by sulphide complexes (Benoit et al., 1999). The effective oxidation of Hg^0 by marine-derived organobromines and the complexing of Hg by organics and sulphides in the oceans establishes marine sediments as an efficient sink of atmospheric Hg (Benoit et al., 1999; Emili et al., 2011; Horowitz et al., 2017). Therefore, marine siliciclastic and carbonate rocks can act as an important repository of Hg during times of heightened environmental loading (Percival et al., 2015; Grasby et al., 2016). It is also worth noting that once in the atmosphere particulate Hg can also be removed via “dry deposition”, a portion of which may make its way into the terrestrial realm (see Munthe et al., 2009 for discussion).

The Cambrian Period is marked by large oscillations of the inorganic carbon isotope record which, at times, coincided with intensified extinction rates (Brasier et al., 1994; Montañez et al., 2000; Zhu et al., 2006). At the Cambrian Series 2 – Series 3 boundary, a negative $\delta^{13}C$ excursion referred to as the Redlichiid – Olenellid Extinction Carbon isotope Excursion (ROECE) has been documented from Laurentia (Montańez, 2000; Faggetter et al., 2017), Gondwana (Schmid, 2017) and China (e.g. Fan et al., 2011; Wang et al., 2011; Chang et al., 2017; Ren et al., 2017). This coincides with major trilobite losses in both Gondwana and Laurentia (Montañez et al., 2000; Zhu et al., 2004; 2006; Faggetter et al., 2017; Ren et al., 2017). The Series 2 – Series 3 boundary age (~509 Ma, Ogg et al., 2016) approximately coincides with the 510.7 ± 0.6 Ma age of the Kalkarindji Province (Jourdan et al., 2014) but detailed correlation is lacking. We attempt to resolve this issue by examining sedimentary Hg concentrations in Cambrian Series 2 – Series 3 sections of the western USA. We have analysed Hg concentrations and Hg/ total organic carbon content (TOC) from two formations and three sections in the western Great Basin: Carrara Formation, Emigrant Pass (Death Valley, CA) and the Pioche Formation at Oak Springs Summit and Ruin Wash (Lincoln County, NV). These sections have an established biostratigraphic framework, and also a record of trilobite extinction at Oak Springs Summit and Ruin Wash (Webster et al., 2008; Moore and Lieberman, 2009).

2. STUDY AREA

Cambrian successions of the western Great Basin (USA) constitute the primary field locations of this study. Following the breakup of the supercontinent Rodinia in the late Neoproterozoic, a broad, equatorial clastic shelf developed on the rapidly subsiding Laurentian margin (Prave, 1991; Howley et al., 2006). During Cambrian Series 2, deposition in the Great Basin was on a broad shelf located on the north-western margin of Laurentia (Fig. 1). Clastic deposition was waning and, by Series 3, it had been replaced by carbonate production, resulting in the formation of an extensive carbonate shelf (Fig. 1; Howley et al., 2006; Landing, 2012). We present data from two formations spanning the Cambrian Series 2 – Series 3 boundary in the western Great Basin. The first section records the Carrara Formation of Death Valley, exposed at Emigrant Pass, California (Fig. 2). The second section is the Pioche Formation of eastern Nevada exposed at Oak Springs Summit (Fig. 3), and a third section at Ruin Wash, also recording the Pioche Formation (Fig. 4). Oak Springs Summit and Ruin Wash are close to each other (~20kms apart), whilst Emigrant Pass is ~225km south-west of these two locations (Fig. 1). Both formations comprise alternating siliciclastic- and limestone-dominated units (Merriam and Palmer, 1964; Palmer and Halley, 1979; Faggetter et al., 2017). At Oak Springs Summit and Ruin Wash, the Pioche Formation records the abrupt extinction of the olenellid trilobites, making these two sections candidates for paired Hg-biostratigraphic studies. At Emigrant Pass there is a paucity of trilobite fossils, but $\delta^{13}C$ correlation, based on the record of the ROECE (e.g., Zhu et al., 2004), allows an extinction interval to be inferred at the boundary between the Olenellus and Eokochaspis nodosa biozones in the mid Pyramid Shale (Fig, 2; Faggetter et al., 2017). As a further stratigraphic tie point between the two formations, the extinction horizon within the Pioche Formation represents the top of the Olenellus biozone (Palmer, 1998; Sundberg and McCollum, 2000).

3. METHODS

We analysed total Hg content in whole-rock powders from 93 samples taken from the three Series 2 – Series 3 boundary sections in the western US (Figs. 2, 3, 4). The samples from Emigrant Pass and Oak Springs Summit were run at the Geological Survey of Canada with a LECO® AMA254 mercury analyser (10% precision, 5% relative standard deviation (RSD), Hall and Pelchat, 1997). Whole rock powders from Ruin Wash, as well as a duplicate sample set from Oak Springs Summit, were analysed at Amherst College (Massachusetts, USA) using a Teledyne Leeman Labs Hydra II$_C$ mercury analyser (RSD <10%). Duplicate samples returned a correlation coefficient of 0.99, indicating a robust positive correlation between the results from the two laboratories.

Whole-rock powders were decarbonated using hydrochloric acid, and their carbonate content was calculated by mass loss following acid digestion. With the exception of Ruin Wash samples, TOC was measured from insoluble residues at the

University of Leeds using a LECO® SC-144DR Dual Range carbon and sulphur analyser. The carbon content of insoluble residues from Ruin Wash was measured with a Costech ECS 4010 elemental analyser at Amherst College in order to generate TOC measurements, with RSD <5%.

Inorganic carbon isotope values from the Carrara Formation at Emigrant Pass and Pioche Formation, Oak Springs Summit are reproduced from Faggetter et al. (2017), and new inorganic carbon isotope values from Ruin Wash are presented here. Whole-rock powders were analysed at the GeoZentrum Nordbayern, FAU Erlangen-Nuremberg, Germany, where carbon dioxide was prepared via reaction with phosphoric acid at 70℃ using a Gasbench II preparation system; carbon isotope ratios were measured by a ThermoFisher Delta V plus mass spectrometer in continuous flow mode. Isotope ratios are reported relative to the V-PDB standard, with a reproducibility of ±0.06‰ for $\delta^{13}C$ and 0.05‰ for $\delta^{18}O$.

Inferred redox conditions (Figs. 2, 3, 4) are based upon pyrite framboid size distribution as reported in Faggetter et al. (2017); samples were assessed using a scanning electron microscope (FEI Quanta 650 FEG-ESEM) in backscatter mode following Bond and Wignall (2010).

4. RESULTS

4.1. TOC concentrations

Throughout all three sections TOC content is generally very low and exhibits correlation with facies (Fig. 5). The lowest TOC values (<0.15 wt% TOC) of all three sections are found in marl facies that coincide with extremely low/carbonate free intervals such as the C-Shale Member of the Pioche Formation (Fig. 5). In the Pioche Formation, higher TOC values are preserved in limestone of the Combined Metals Member, at Oak Springs Summit where levels reach 0.48 – 2.69 wt% within an oncoidal limestone of the Combined Metals Member (Fig. 5). The majority of the Carrara Formation is composed of marl with very low (<0.15 wt%) TOC content, the exception being horizons within the Echo Shale and Gold Ace members where values span the greatest range of all three sections (<0.15 – 5.17 wt% TOC) (Fig. 5).

4.2. The ROECE and trilobite extinction

The inorganic carbon isotope record from the Carrara Formation at Emigrant Pass and the Pioche Formation at Oak Springs Summit are discussed in Faggetter et al. (2017) in which a C isotope excursion of ~-3.8 ‰ is interpreted to be the ROECE. Within the Pioche Formation at Oak Springs Summit, the most negative inorganic carbon isotope values coincide with the extinction horizon of the olenellid trilobites. ROECE is also expected to occur at Ruin Wash (Palmer 1998; Faggetter et al., 2017), but the extremely low carbonate content (below detection limits) in the shale of the C-Shale Member at this location does not allow measurement of a continuous inorganic carbon isotope curve. The ROECE is also observed within the Pyramid Shale Member of the Carrara Formation, but unlike the Pioche Formation, there is no trilobite fauna to delineate a clear extinction horizon at Emigrant Pass (Fig. 2). An inferred extinction interval is therefore proposed at Emigrant Pass within the Pyramid Shale Member (Fig. 2), based on the biostratigraphic boundary between the Olenellus Zone and the Eokochaspis nodosa Zone (Fig. 2; see Palmer and Halley, 1979; Faggetter et al, 2017).

4.3. Hg concentrations, Hg/TOC ratios and extinction

The Carrara and Pioche formations contain enrichments in Hg concentrations (ppb) and excursions in Hg/TOC (ppb/wt% TOC) ratios (Figs. 2, 3, 4). Hg/TOC ratios from samples with extremely low TOC of <0.01 wt% C are not considered robust enough to record a primary Hg signal and are not plotted in figures but are included in Table 1.

4.3.1. Carrara Formation, Emigrant Pass

The Carrara Formation at Emigrant Pass exhibits background Hg concentrations of <50 ppb throughout the section (Fig. 2). High Hg and Hg/TOC values are seen in samples with both high and low TOC wt% values (Fig. 6). A number of prominent enrichments occur in the lowest 90 m, with the most enriched sample containing 270 ppb Hg found in the basal Eagle Mountain Shale Member. Smaller enrichments recorded by one or two data points each occur in the Echo Shale, Gold Ace and Pyramid Shale members. Within the ROECE interval Hg values are elevated at the beginning of the $\delta^{13}C$ excursion before concentrations return to low levels for the remainder of the section.

The Hg/TOC enrichments in the Carrara Formation occur in two distinct pulses where Hg and Hg/TOC peaks correlate; an initial, multi-peak enrichment in the basal 30m of the Eagle Mountain Shale Member and another during early

ROECE at the base of the Pyramid Shale Member (Fig. 2). It is noteworthy that across the inferred extinction horizon, there are no abrupt Hg or Hg/TOC peaks and values remain stable in this interval.

4.3.2. Pioche Formation, Oak Springs Summit

Background Hg concentrations in the Pioche Formation at Oak Springs Summit are <10 ppb (Fig. 3). Highest Hg values coincide with samples with low (<0.1 wt%) TOC (Figs. 5 and 6). A single elevated value (46 ppb Hg) occurs in the Combined Metals Member, just below the base of the ROECE, and a smaller enrichment (32 ppb Hg) coincides with the most negative ROECE value and the olenellid extinction horizon at the base of the C-Shale Member. Finally, there is a small increase in Hg concentration (17 ppb) at ~35m in the section, which, like the other enrichments, correspond to three prominent Hg/TOC spikes at Oak Springs Summit (Fig. 3).

4.3.3. Pioche Formation, Ruin Wash

High Hg and Hg/TOC values are recorded in samples with both high and low TOC wt% values (Fig. 6) at Ruin Wash. The Hg values are highest (up to 500 ppb) at the base of the measured section in the basal ~5m of the Combined Metals Member (Fig. 4). Peaks are around an order of magnitude higher than the maximum values seen at Oak Springs Summit. Above the level of elevated values at Ruin Wash, Hg concentrations are consistently <5 ppb, and there is no increase at the olenellid extinction horizon.

5. DISCUSSION

The three sections show an inconsistent correspondence between the olenellid trilobite extinction, ROECE and sedimentary Hg enrichments (Fig. 7). We review possible points for correlation between sections (e.g. ROECE interval and the trilobite extinction) and discuss processes which may account for the variable Hg signal.

5.1. ROECE, Hg and Hg/TOC correlation

To assess any correlation between the timing of Hg enrichment and ROECE, we delineate the base of the excursion based on the following two criteria. Firstly, the onset of ROECE should be present within the Pyramid Shale Member of the Carrara Formation and the upper Combined Metals Member of the Pioche Formation; this is based on an abrupt negative carbon isotope excursion within the Olenellus trilobite biozone, immediately preceding the olenellid extinction (Montañez et al., 2000). Secondly, given this stratigraphic constraint, we mark the onset of the excursion as the stratigraphic base of the negative inflexion interpreted within these members, i.e. ~60 m at Emigrant Pass and ~13 m at Oak Springs Summit. Between the Carrara and Pioche formations, our data show no clear relationship between the onset of ROECE and Hg or Hg/TOC enrichments. At Emigrant Pass an enrichment occurs around 10 m above the base of ROECE and at Oak Springs Summit an enrichment occurs ~1 m below the base of the excursion. It is clear from enrichments in the Eagle Mountain Shale Member of the Carrara Formation and in the Combined Metals Member of the Pioche Formation that the majority of Hg and Hg/TOC excursions occur before the ROECE interval.

5.2. Extinction, Hg and Hg/TOC

In the Pioche Formation at Oak Springs Summit, a small Hg (32 ppb, compared to a background of <5ppb for this section) and Hg/TOC excursion corresponds closely with the extinction horizon and the top of the Olenellus biozone (Fig. 7). However, the relationship between olenellid extinction and Hg or Hg/TOC enrichment is inconsistent among the other studied sections (Figs. 3 and 7). There is no enrichment coincident with the top of the Olenellus biozone at Emigrant Pass, nor at the extinction horizon at Ruin Wash (Fig. 7).

The high levels of Hg enrichment are generally recorded low in the study sections. In the Combined Metals Member at Ruin Wash, this is seen ~15 and ~10m below the olenellid extinction level at Ruin Wash (Fig. 4), and even lower below this level at Emigrant Pass (Fig. 2). Based on the lithostratigraphic correlation of Palmer (1998), it is unlikely that the levels of Hg enrichment can be correlated with each other (Fig. 7).

The inconsistency of the relationship between Hg, ROECE and extinction across all three sections challenges the conventional use of Hg as a tracer for global environmental Hg loading in this case. Previous Hg chemostratigraphic profiles invoked to trace global LIP eruptions predict, and exhibit, synchronous Hg signals across regional and global sites (e.g. Percival et al., 2017). The lack of a reproducible Hg signal across our sections precludes a straightforward interpretation of the Hg chemostratigraphy. Our data show that only at Emigrant Pass does the base of ROECE coincide with Hg enrichment, but not the duration of the isotopic excursion. There is no Hg enrichment across the extinction interval.

The observed heterogeneity of enrichments in Hg and Hg/TOC values could be caused by several factors related to environmental and diagenetic processes. Our data demonstrate that volcanic loading and binding to organic matter cannot be the sole drivers of the Hg record in these strata. We therefore consider the possible roles that redox variations and binding to clays (and possibly sulphides) may have played in controlling Hg levels.

5.3. Hg enrichments, redox variation and TOC

Previous studies have exhibited limited correlation between redox conditions, organic matter deposition and Hg drawdown (e.g. Grasby et al., 2013; Percival et al., 2015). However, studies from the modern suggest the redox state of the sediment and water column can play an important role in mobilising or re-mobilising Hg species and enhancing or diminishing Hg exchange between the sediment and water column (Mason et al., 2006; Emili et al., 2011). Mercury and methyl mercury (MeHg) are scavenged in oxic conditions and sequestered in the sediments; however, the upward migration of the redox boundary causes Hg and MeHg to be released into the water column (Emili et al., 2011; Yin et al., 2017). Emili et al. (2011) modelled Hg cycling between the sediment and water column under anoxic conditions and showed a strong redox control on the mobility of Hg. They found that benthic Hg flux from the sediment to water column is highest during anoxic conditions and is also accentuated during sulfate reduction in euxinic conditions.

Assessment of redox states within the Carrara and Pioche formations found intermittent and locally variable periods of dysoxia during the olenellid extinction interval (Webster et al., 2008; Faggetter et al., 2017). Pyrite petrography shows dominantly oxygenated conditions (i.e. no framboids, scarce pyrite crystals) at Emigrant Pass (Fig. 2), variably oxygenated-dysoxic-euxinic conditions at Oak Springs Summit close to the extinction horizon (Fig. 3) and, euxinic to oxygenated conditions across the extinction horizon at Ruin Wash (Fig. 4) (Faggetter et al.

2017). These fluctuating redox conditions could have altered drawdown of Hg from the water column to the sediments (Horowitz et al., 2017) during times of heightened Hg loading. The euxinic pyrite framboid size data from two samples at the Ruin Wash trilobite extinction level do not correspond with Hg enrichment. Thus, the varying behaviour of Hg under different redox conditions could underlie the differing relationship between Hg and extinction in the Pioche Formation.

It is important to note that previously published studies reporting Hg sedimentary trends across multiple sections similarly reveal variable Hg and Hg/TOC ranges between localities (e.g. Grasby et al., 2016; Jones et al., 2017). Such discrepancies may be an inherent component of volcanically-derived deposition and fixation in marine sediments. For instance, a variable record of Hg enrichment during anoxia-related extinction is reported during the Toarcian (Early Jurassic) extinction (Percival et al., 2015). This event coincides with the organic-rich shales of the Jet Rock in northern England, but these sediments lack the Hg enrichment that otherwise might be expected given contemporaneous eruption of the Karoo-Ferrar flood basalt province. Percival et al. (2015) argue that efficient organo-Hg scavenging in organic-rich euxinic settings may have caused over-printing of the Hg/TOC anomaly by excess organic matter deposition. However, such a mechanism is unlikely in our reported Cambrian examples because TOC values in the C-Shale at Ruin Wash are low (<0.3 wt %; Fig. 5). The Carrara and Pioche formations are similarly characterised by low TOC and a range of Hg concentrations and Hg/TOC values; we interpret this signature as showing that even in organic-poor rocks it is possible to record elevated Hg concentrations during times of heightened environmental loading (Figs. 5 and 6), a conclusion drawn from other organic-lean records (e.g. Font et al., 2016; Percival et al., 2017). At Oak Springs Summit Hg and Hg/TOC excursions occur in samples containing low TOC (<0.15 wt% C), whilst at Emigrant Pass and Ruin Wash enrichments occur across a range of wt% TOC values (Fig. 6). The absence of a strong correlation between Hg and TOC (Fig. 5) at all three sections therefore indicates that Hg enrichment is not a function of variable TOC; we therefore posit that these anomalies are not solely a function of low TOC.

5.4. Hg and mineralogy

Hg accumulation may also be controlled in part by binding to phases other than organic matter. The samples analysed here exhibit very low TOC (wt%) values and commonly comprise marl facies. Because clay minerals can act as an efficient Hg binding medium in the absence of a larger organic matter reservoir, the sediment/rock composition at the time of Hg deposition may partially control Hg concentration (Zhong and Wang, 2008; Kongchum et al., 2011). High surface area reactivity for clay minerals make them effective regulators of Hg in aquatic sediments and up to an order of magnitude higher Hg concentrations have been found in secondary minerals such as clay versus primary minerals such as quartz and feldspar (Tessier et al., 1982). Higher proportions of primary silicate minerals therefore have the capability to “dilute” the amount of Hg binding during Hg loading (Tessier et al., 1982), and a variation in sediment composition across our study location could be a contributing factor to the observed inconsistent Hg records.

5.5. Hg as an indicator of volcanism

The pre-ROECE levels of Hg enrichment observed at Emigrant Pass and Ruin Wash are enigmatic, and it is currently unclear if they record an unknown local volcanic source, an early eruptive pulse of the Kalkarindji LIP, or are instead a response to sedimentary/diagenetic redox variations. To resolve this uncertainty, further work is required to determine how widespread these perturbations are, both within Laurentia and globally.

Challenges to linking Hg excursions with LIP volcanism are not restricted to our Cambrian successions. Percival et al. (2018) present a comprehensive comparison of Hg records from the Mesozoic, focussing on the coincidence of LIP emplacement and ocean anoxic events, and report variable (both in Hg and Hg/TOC) concentrations across sections and lithologies and also contrasting evidence of Hg enrichment during periods of LIP volcanism (e.g. an absence of a broad global Hg excursion during Deccan volcanism contrasting with osmium-isotope records). The apparent inconsistency between these proxies is likely due to the various environments, lithologies and depositional processes.

Although the lack of consistent Hg records between the analysed sections prevents arguing definitively for a link between Kalkarindji and the extinction event at this stage, it remains likely that some of the recorded Hg excursions do record an expression of these LIP eruptions for the following reasons:

- The Kalkarindji LIP lacks a robust body of radiometric dates, Accordingly, additional dating efforts within the Kalkarindji province itself may also help clarify its emplacement history, and whether initial volcanic pulses occurred considerably earlier than current geochronological constraints suggest. Current age dating does suggest that the onset of eruption may straddle, or possibly predates the Series 2 – Series 3 boundary (Marshall et al., 2018), thus raising the possibility that the Hg record from the Great Basin records other volcanic eruptions. If this proves to be the case, then Hg anomalies may be a useful marker for independently implicating specific volcanic events, but offers limited resolution when attempting to discriminate between multiple contemporaneous sources.

- Many LIPs, whilst erupted rapidly on a geological timescale, are iterative in their eruptive behaviour and being characterised by short periods of very intense activity (Chenet et al., 2008; Vye-Brown et al., 2013). For instance, high-resolution geochronological studies have revealed that eruptions of other large igneous provinces occur in a pulsed nature, particularly the Permo-Triassic Siberian Traps (Burgess et al., 2017), the end-Triassic Central Atlantic Magmatic Province (Davies et al., 2017) and the end-Cretaceous Deccan Traps (Schoene et al., 2015). Given the evidence for pulsed LIP emplacement throughout Earth history, it is plausible that multiple eruption episodes characterise the emplacement of the Kalkarindji LIP.
- The broad-scale architecture of the province, as evidenced by the several geochemically related sub-provinces (Glass and Phillips, 2006), may indicate more than one eruptive focus during its eruptive lifetime.
- Marshall et al. (2016) report that many Kalkarindji flows were effectively degassed: such near-complete degassing could have occurred either at the vent source (Guilbaud et al., 2007) or during propagation across the evolving lava fields. Importantly, degassing occurs either during fissure eruption and associated fire-fountaining similar to that observed from Laki eruptions. Such effusions can transport volcanogenic volatiles high into the troposphere, and possibly into the stratosphere, since fire fountains, augmented by heat released from nascent flows drive thermal uplift generating buoyant ash and gas plumes (Thordarson and Self, 1998; Glaze et al., 2017). Accordingly, volatiles may be lofted high into the atmosphere (Stothers et al., 1986; Woods, 1993), and this available for distribution certainly at local and regional

scales or, under favourable conditions, more globally. In this context, it is important to note that the Kalkarindji LIP was erupted near the equator (Fig. 1; Cocks and Torsvik, 2013; Lawver et al., 2015) where the tropopause would have been at a greater altitude thus mitigating against wider distribution, but that atmospheric circulation patterns an equatorial location would have otherwise aided in allowing aerosol distribution to both hemispheres

- In addition, Marshall et al., (2016) also argue for a fundamental change in eruptive style; the main succession being typified by thick, inflated pahoehoe flow and the overlying Blackfella Rockhole Member (BRM), which is instead characterised by huge rubble-topped flows. This change in eruptive style, together the occurrence of stromatolite reefs and aeolian(?) sand horizons preserved within these upper eruptive units indicates that later eruptive episodes occurred into a complex paleoenvironment affected by both terrestrial and shallow marine conditions.

To summarise, the degree and timing of Hg release is likely to have varied significantly during construction of the Kalkarindji LIP and, together with outlined factors controlling lofting and circulation of volatiles, may thus help explain the iterative and/or incomplete record of Hg here reported in the mid-Cambrian marine sediments.

6. CONCLUSION

We report sedimentary Hg and Hg/TOC enrichments from both the Carrara and Pioche formations of the western Great Basin, USA. These successions are constrained within a biostratigraphic and chemostratigraphic framework to record the Cambrian Series 2 – Series 3 boundary, and the extinction of the Laurentian olenellid trilobites is observable within the Pioche Formation. The ROECE is present at two of the three studied sections (Emigrant Pass, Carrara Formation and Oak Springs Summit, Pioche Formation). In the Carrara Formation, the majority of Hg enrichments predate ROECE, with a single enrichment occurring just above the base of the excursion. At Oak Springs Summit ROECE is preceded by Hg enrichment.

Within the Pioche Formation at Oak Springs Summit the extinction horizon of the olenellid trilobites is marked by positive Hg and Hg/TOC excursions; however, a similar excursion is not apparent at the equivalent horizon from Ruin Wash. The failure to locate Hg enrichment in the euxinic Ruin Wash section suggest that the redox conditions were unfavourable. Our data supports the hypothesis that Hg and Hg/TOC enrichments within the Carrara and Pioche formations are not solely derived from enhanced TOC preservation, but that inconsistent Hg trends may have resulted from variable environmental and diagenetic processes at the different sites. Given the strong control anoxia exerts on Hg flux, speciation and accumulation in modern settings, the role of redox states in deep time is clearly important when assessing the record of Hg in rocks.

The timing, volume and palaeo-position of the Kalkarindji LIP makes it a key candidate as the source of environmental Hg loading and subsequent enrichments in the Carrara and Pioche formations. Thus, the Kalkarindji potentially contributed to the Hg concentrations at the Cambrian Series 2 – Series 3 boundary, and that the occurrence of precursor levels of Hg enrichment may point to hitherto unrecognised phases of volcanism during construction of the Kalkarindji LIP, or else the possibility of other, as yet, unknown major volcanic episodes.

ACKNOWLEDGMENTS

LF was funded by a Natural Environment Research Council doctoral training grant at Leeds University. We thank Michael Joachimski and Yadong Sun for the use of their stable isotope lab at the Friedrich-Alexander Univesität, Erlangen-Nürnberg, and Maria Kopicki for laboratory assistance at Amherst College. We also thank A.N. Sial and one anonymous reviewer for their helpful feedback during the peer-review process.

REFERENCES CITED

Chenet, A. L., Courtillot, V., Fluteau, F., Gérard, M., Quidelleur, X., Khadri, S. F. R., Thordarson, T. (2009). Determination of rapid Deccan eruptions across the Cretaceous-Tertiary boundary using paleomagnetic secular variation: 2. Constraints from analysis of eight new sections and synthesis for a 3500-m-thick composite section. Journal of Geophysical Research: Solid Earth, 114(B6).

Benoit, J.M., Gilmour, C.C., Mason, R.P., Heyes, R., (1999). Sulfide controls on mercury speciation and bioavailability to methylating bacteria in sediment pore

waters. Environ. Sci. Technol. 33, 951–957.
Benoit, J.M., Mason, R.P., Gilmour, C.C., Aiken, G.R., (2001). Constants for mercury binding by dissolved organic matter isolates from the Florida Everglades. Geochim. Cosmochim. Acta 65, 4445–4451.
Bergquist, B. A. (2017). Mercury, volcanism, and mass extinctions. Proceedings of the National Academy of Sciences, 114(33), 8675-8677.
Blackburn, T. J., Olsen, P. E., Bowring, S. A., McLean, N. M., Kent, D. V., Puffer, J., Et-Touhami, M. (2013). Zircon U-Pb geochronology links the end-Triassic extinction with the Central Atlantic Magmatic Province. Science, 340(6135), 941-945.
Bond, D. P., Wignall, P. B. (2010). Pyrite framboid study of marine Permian–Triassic boundary sections: a complex anoxic event and its relationship to contemporaneous mass extinction. Geological Society of America Bulletin, 122(7-8), 1265-1279.
Brasier, M. D., Corfield, R. M., Derry, L. A., Rozanov, A. Y., Zhuravlev, A. Y. (1994). Multiple δ13C excursions spanning the Cambrian explosion to the Botomian crisis in Siberia. Geology, 22(5), 455-458.
Burgess, S. D., Muirhead, J. D., Bowring, S. A. (2017). Initial pulse of Siberian Traps sills as the trigger of the end-Permian mass extinction. Nature communications, 8(1), 164.
Chang, C., Hu, W., Wang, X., Yu, H., Yang, A., Cao, J., Yao, S. (2017). Carbon isotope stratigraphy of the lower to middle Cambrian on the eastern Yangtze Platform, South China. Palaeogeography, Palaeoclimatology, Palaeoecology, 479, 90-101.
Cocks, L. R. M. and Torsvik, T.M. (2013). The dynamic evolution of the Palaeozoic geography of eastern Asia. Earth-Science Reviews 117: 40-79.
Courtillot, V. E., & Renne, P. R. (2003). On the ages of flood basalt events. Comptes Rendus Geoscience, 335(1), 113-140.
Dal Corso, J., Marzoli, A., Tateo, F., Jenkyns, H. C., Bertrand, H., Youbi, N., Cirilli, S. (2014). The dawn of CAMP volcanism and its bearing on the end-Triassic carbon cycle disruption. Journal of the Geological Society, 171(2), 153-164.
Davies, J. H. F. L., Marzoli, A., Bertrand, H., Youbi, N., Ernesto, M., Schaltegger, U. (2017). End-Triassic mass extinction started by intrusive CAMP activity. Nature communications, 8, 15596.

Emili, A., Koron, N., Covelli, S., Faganeli, J., Acquavita, A., Predonzani, S., De Vittor, C. (2011). Does anoxia affect mercury cycling at the sediment–water interface in the Gulf of Trieste (northern Adriatic Sea)? Incubation experiments using benthic flux chambers. Applied geochemistry, 26(2), 194-204.

Ernst, R.E. and Youbi, N. (2017). How large igneous provinces affect global climate, sometimes cause mass extinction, and represent natural markers in the geological record. Palaeogeography, Palaeoclimatology, Palaeoecology. 478, 30-52

Faggetter, L.E., Wignall, P.B., Pruss, S.B., Newton, R.J., Sun, Y.D. and Crowley, S. (2017). Trilobite extinctions, facies changes and the ROECE carbon isotope excursion at the Cambrian Series 2-3 boundary, Great Basin, western USA. Palaeogeography, Palaeoclimatology, Palaeoecology, 478, 53-66

Fan, R., Deng, S., Zhang, X. (2011). Significant carbon isotope excursions in the Cambrian and their implications for global correlations. Science China Earth Sciences, 54(11), 1686-1695.

Fitzgerald, W.F., Lamborg, C.H., Hammerschmidt, C.R. (2007). Marine biogeochemical cycling of mercury. Chemical Reviews. 107, 641–662

Font, E., Adatte, T., Sial, A. N., de Lacerda, L. D., Keller, G., Punekar, J. (2016). Mercury anomaly, Deccan volcanism, and the end-Cretaceous mass extinction. Geology, 44(2), 171-174.

Glass, L. M., Phillips, D. (2006). The Kalkarindji continental flood basalt province: A new Cambrian large igneous province in Australia with possible links to faunal extinctions. Geology, 34(6), 461-464.

Glaze, L. S., Self, S., Schmidt, A., Hunter, S. J. (2017). Assessing eruption column height in ancient flood basalt eruptions. Earth and Planetary Science Letters, 457, 263-270.

Gong, Q., Wang, X., Zhao, L., Grasby, S. E., Chen, Z. Q., Zhang, L., Li, Z. (2017). Mercury spikes suggest volcanic driver of the Ordovician-Silurian mass extinction. Scientific Reports, 7.

Grasby, S.E., Sanei, H., Beauchamp, B., Chen, Z. (2013). Mercury deposition through the Permo–Triassic biotic crisis. Chemical Geology, 351, 209-216.

Grasby, S.E., Beauchamp, B., Bond, D.P.G., Wignall, P.B., Sanei, H. (2016). Mercury anomalies associated with three extinction events (Capitanian crisis, latest Permian extinction and the Smithian/Spathian extinction) in NW

Pangea. Geological Magazine 153, 285-297. doi:10.1017/S0016756815000436

Hall, G. E., Pelchat, P. (1997). Evaluation of a direct solid sampling atomic absorption spectrometer for the trace determination of mercury in geological samples. Analyst, 122(9), 921-924.

Horowitz, H. M., Jacob, D. J., Zhang, Y., Dibble, T. S., Slemr, F., Amos, H. M., Sunderland, E. M. (2017). A new mechanism for atmospheric mercury redox chemistry: Implications for the global mercury budget. Atmospheric Chemistry and Physics, 17(10), 6353-6371.

Hough, M.L., Shields, G.A., Evins, L.Z., Strauss, H., Henderson, R.A., Mackenzie, S. (2006). A major Sulphur isotope evnt at c. 510 Ma: a possible anoxia-extinction-volcanism connection during the Early-Middle Cambrian transition? Terra Nova 18, 257-263. doi: 10.1111/j.1365-3121.2006.00687.x

Howley, R.A., Rees, M. N., Jiang, G. (2006). Significance of Middle Cambrian mixed carbonate-siliciclastic units for global correlation: southern Nevada, USA. Palaeoworld, 15(3), 360-366.

Jones, D. S., Martini, A. M., Fike, D. A. Kaiho, K. (2017). A volcanic trigger for the Late Ordovician mass extinction? Mercury data from south China and Laurentia. Geology, 45(7), 631-634.

Jourdan, F., Hodges, K., Sell, B., Schaltegger, U., Wingate, M.T. D., Evins, L.Z., Blenkinsop, T. (2014). High-precision dating of the Kalkarindji large igneous province, Australia, and synchrony with the Early–Middle Cambrian (Stage 4–5) extinction. Geology, 42(6), 543-546.

Kongchum, M., Hudnall, W. H., Delaune, R. D. (2011). Relationship between sediment clay minerals and total mercury. Journal of Environmental Science and Health, Part A, 46(5), 534-539.

Kravchinsky, V.A. (2012). Paleozoic large igneous provinces of Northern Eurasia: Correlation with mass extinction events. Glob. Planet. Change 86–87, 31–36. doi:10.1016/j.gloplacha.2012.01.007

Landing, E. (2012). The great American carbonate bank in eastern Laurentia: Its births, deaths, and linkage to paleooceanic oxygenation (Early Cambrian – Late Ordovician), in J. R. Derby, R. D. Fritz, S. A. Longacre, W. A. Morgan, and C. A. Sternbach, eds., The great American carbonate bank: The geology and economic resources of the Cambrian – Ordovician Sauk megasequence of Laurentia: AAPG Memoir 98, p. 451 – 492.

Lawver, L.A., Dalziel, I.W.D., Norton, I.O., Gahagan, L.M., Davis, J., (2015). The PLATES 2014 Atlas of Plate Reconstructions (550 Ma to Present Day), PLATES Progress Report No. 374-0215, University of Texas Technical Report No. 201, 220p.

Li, Z. X., Zhang, L., Powell, C. M. (1996). Positions of the East Asian cratons in the Neoproterozoic supercontinent Rodinia. Australian Journal of Earth Sciences, 43(6), 593-604.

Li, Z. X., Bogdanova, S. V., Collins, A. S., Davidson, A., De Waele, B., Ernst, R. E., Karlstrom, K. E. (2008). Assembly, configuration, and break-up history of Rodinia: a synthesis. Precambrian Research, 160(1), 179-210.

Marshall, P. E., Widdowson, M., Murphy, D. T. (2016). The Giant Lavas of Kalkarindji: rubbly pāhoehoe lava in an ancient continental flood basalt province. Palaeogeography, Palaeoclimatology, Palaeoecology, 441, 22-37.

Marshall, P. E., Halton, A. M., Kelley, S. P., Widdowson, M., Sherlock, S. C. (2018). New 40Ar/39Ar dating of the Antrim Plateau Volcanics, Australia: clarifying an age for the eruptive phase of the Kalkarindji continental flood basalt province. Journal of the Geological Society, 2018-035.

Mason, R. P., Fitzgerald, W. F., Hurley, J., Hanson, A. K., Donaghay, P. L., Sieburth, J. M. (1993). Mercury biogeochemical cycling in a stratified estuary. Limnology and Oceanography, 38(6), 1227-1241.

Mason, R. P., Kim, E. H., Cornwell, J., Heyes, D. (2006). An examination of the factors influencing the flux of mercury, methylmercury and other constituents from estuarine sediment. Marine Chemistry, 102(1-2), 96-110.

Merriam, C. W., Palmer, A. R. (1964). Cambrian rocks of the Pioche mining district, Nevada, with a section on Pioche shale faunules (No. 469). United States Geological Survey Professional Paper, 569, 59

Monperrus, M., Tessier, E., Amouroux, D., Leynaert, A., Huonnic, P., Donard, O. F. X. (2007). Mercury methylation, demethylation and reduction rates in coastal and marine surface waters of the Mediterranean Sea. Marine Chemistry, 107(1), 49-63.

Montañez, I. P., Osleger, D. A., Banner, J. L., Mack, L. E., Musgrove, M. (2000). Evolution of the Sr and C isotope composition of Cambrian oceans. GSA Today, 10(5), 1-7.

Moore, R. A., Lieberman, B. S. (2009). Preservation of early and Middle Cambrian soft-bodied arthropods from the Pioche Shale, Nevada, USA. Palaeogeography, Palaeoclimatology, Palaeoecology, 277(1), 57-62.

Munthe, J., Wängberg, I., & Shang, L. (2009). The origin and fate of mercury species in the natural environment. Eur. Chlor. Sci. Doss, 14.

Ogg, J. G., Ogg, G., Gradstein, F. M. (2016). A Concise Geologic Time Scale: 2016. Elsevier.

Palmer, A.R. (1998). Terminal early Cambrian extinction of the Olenellina: documentation from the Pioche Formation, Nevada. Journal of Paleontology, 72 (04), 650-672.

Palmer, A. R., Halley, R. B. (1979). Physical stratigraphy and trilobite biostratigraphy of the Carrara Formation (Lower and Middle Cambrian) in the southern Great Basin (No. 1047). United States Geological Survey Professional Paper, 1047, 113p

Payne, J.L., Lehrmann, D.J., Wei, J., Orchard, M.J., Schrag, D.P., Knoll, A.H. (2004). Large perturbations of the carbon cycle during recovery from the end-Permian extinction. Science 305 (5683), 506–509.

Percival, L.M.E., Witt, M.L.I., Mather, T.A., Hermoso, M., Jenkyns, H.C., Hesselbo, S.P., Al-Suwaidi, A.H., Storm, M.S., Xu, W., Ruhl, M. (2015). Globally enhanced mercury deposition during the end-Pliensbachian extinction and Toarcian OAE: A link to the Karoo-Ferrar Large Igneous Province. Earth ad Planetary Science Letters 428, 267-280.

Percival, L. M., Ruhl, M., Hesselbo, S. P., Jenkyns, H. C., Mather, T. A., Whiteside, J. H. (2017). Mercury evidence for pulsed volcanism during the end-Triassic mass extinction. Proceedings of the National Academy of Sciences, 114(30), 7929-7934.

Percival, L. M., Jenkyns, H. C., Mather, T. A., Dickson, A. J., Batenburg, S. J., Ruhl, M., Woelders, L. (2018). Does large igneous province volcanism always perturb the mercury cycle? Comparing the records of Oceanic Anoxic Event 2 and the end-Cretaceous to other Mesozoic events. American Journal of Science, 318(8), 799-860.

Prave, A.R. (1991). Depositional and sequence stratigraphic framework of the Lower Cambrian Zabriskie Quartzite: implications for regional correlations and the Early Cambrian paleogeography of the Death Valley region of California and Nevada. Geological Society of America Bulletin, 104(5), 505-515.

Pyle, D.M., Mather, T.A. (2003). The importance of volcanic emissions for the global atmo spheric mercury cycle: Atmospheric Environment, v. 37, p. 5115–5124, doi:10.1016/j.at- mosenv.2003.07.011.

Ren, Y., Zhong, D., Gao, C., Liang, T., Sun, H., Wu, D., Zheng, X. (2017). High-resolution carbon isotope records and correlations of the lower Cambrian Longwangmiao formation (stage 4, Toyonian) in Chongqing, South China. Palaeogeography, Palaeoclimatology, Palaeoecology.

Sanei, H., Grasby, S., Beauchamp, B. (2012). Latest Permian mercury anomalies. Geology 40, 63–66. http://dx.doi.org/10.1130/G32596.1.

Schuster, P. F., Krabbenhoft, D. P., Naftz, D. L., Cecil, L. D., Olson, M. L., Dewild, J. F., Abbott, M. L. (2002). Atmospheric mercury deposition during the last 270 years: a glacial ice core record of natural and anthropogenic sources. Environmental Science & Technology, 36(11), 2303-2310.

Sial, A. N., Lacerda, L. D., Ferreira, V. P., Frei, R., Marquillas, R. A., Barbosa, J. A., Pereira, N. S. (2013). Mercury as a proxy for volcanic activity during extreme environmental turnover: The Cretaceous–Paleogene transition. Palaeogeography, Palaeoclimatology, Palaeoecology, 387, 153-164.

Sial, A. N., Chen, J., Lacerda, L. D., Peralta, S., Gaucher, C., Frei, R., Pereira, N. S. (2014). High-resolution Hg chemostratigraphy: A contribution to the distinction of chemical fingerprints of the Deccan volcanism and Cretaceous–Paleogene Boundary impact event. Palaeogeography, Palaeoclimatology, Palaeoecology, 414, 98-115.

Schmid, S. (2017). Chemostratigraphy and palaeo-environmental characterisation of the Cambrian stratigraphy in the Amadeus Basin, Australia. Chemical Geology, 451, 169-182.

Schoene, B., Samperton, K. M., Eddy, M. P., Keller, G., Adatte, T., Bowring, S. A., Gertsch, B. (2015). U-Pb geochronology of the Deccan Traps and relation to the end-Cretaceous mass extinction. Science, 347(6218), 182-184.

Stothers, R. B., Wolff, J. A., Self, S., Rampino, M. R. (1986). Basaltic fissure eruptions, plume heights, and atmospheric aerosols. Geophysical Research Letters, 13(8), 725-728.

Sundberg, F. A., McCollum, L. B. (2000). Ptychopariid trilobites of the lower-middle Cambrian boundary interval, Pioche Shale, southeastern Nevada. Journal of Paleontology, 74(4), 604-630.

Tessier, A. Campbell, P. G., Bisson, M. (1982). Particulate trace metal speciation in stream sediments and relationships with grain size: implications for geochemical exploration. Journal of Geochemical Exploration, 16(2), 77-104.

Thibodeau, A.M., Ritterbush, K., Yager, J.A., West, A.J., Ibarra, Y., Bottjer, D.J., Berelson, W.M., Bergquist, B.A., Corsetti, F.A. (2016). Mercury anomalies and the timing of biotic recovery following the end-Triassic mass extinction. Nature Communications 7:11147, doi: 19.1038/ncomms11147

Veevers, J.J. (2001). Atlas of billion-year old earth history of Australia and neighbours in Gondwanaland. GEMOC Press, Sydney, Australia.

Vye-Brown, C., Self, S., & Barry, T. L. (2013). Architecture and emplacement of flood basalt flow fields: case studies from the Columbia River Basalt Group, NW USA. Bulletin of Volcanology, 75(3), 697.

Wang, X., Hu, W., Yao, S., Chen, Q., Xie, X. (2011). Carbon and strontium isotopes and global correlation of Cambrian Series 2-Series 3 carbonate rocks in the Keping area of the northwestern Tarim Basin, NW China. Marine and Petroleum Geology, 28(5), 992-1002.

Webster, M., Gaines, R. R., Hughes, N. C. (2008). Microstratigraphy, trilobite biostratinomy, and depositional environment of the “Lower Cambrian” Ruin Wash Lagerstätte, Pioche Formation, Nevada. Palaeogeography, Palaeoclimatology, Palaeoecology, 264(1), 100-122.

Wignall, P. B. (2001). Large igneous provinces and mass extinctions. Earth-science Reviews, 53(1), 1-33.

Wignall, P.B. (2015). The Worst of Times: How Life on Earth Survived 80 Million Years of Extinction. Princeton University Press.

Woods, A. W. (1993). A model of the plumes above basaltic fissure eruptions. Geophysical Research Letters, 20(12), 1115-1118.

Yin, R., Xu, L., Lehmann, B., Lepak, R. F., Hurley, J. P., Mao, J., Hu, R. (2017). Anomalous mercury enrichment in Early Cambrian black shales of South China: Mercury isotopes indicate a seawater source. Chemical Geology. 467, 159-167.

Zhang, W.H., Shi, X.Y., Jiang, G.Q., Tang, D.J., Wang, X.Q. (2015). Mass-occurrence of oncoids at the Cambrian Series2-Series 3 transition: Implications for microbial resurgence following an Early Cambrian extinction. Gondwana Research 28, 432-450.

Zhong, H., Wang, W. X. (2008). Effects of sediment composition on inorganic mercury partitioning, speciation and bioavailability in oxic surficial sediments. Environmental pollution, 151(1), 222-230.

Zhu, M. Y., Zhang, J. M., Li, G. X., Yang, A. H. (2004). Evolution of C isotopes in the Cambrian of China: implications for Cambrian subdivision and trilobite mass extinctions. Geobios, 37(2), 287-301.

Zhu, M. Y., Babcock, L. E., & Peng, S. C. (2006). Advances in Cambrian stratigraphy and paleontology: integrating correlation techniques, paleobiology, taphonomy and paleoenvironmental reconstruction. Palaeoworld, 15(3), 217-222.

Zhu, D. C., Zhao, Z. D., Niu, Y., Dilek, Y., Wang, Q., Ji, W. H., Mo, X. X. (2012). Cambrian bimodal volcanism in the Lhasa Terrane, southern Tibet: record of an early Paleozoic Andean-type magmatic arc in the Australian proto-Tethyan margin. Chemical Geology, 328, 290-308.

Figure captions

1. Cambrian global palaeogeography at 510 million years ago showing approximate palaeoposition of study sections, adapted from Lawver et al. (2014). Architecture of Kalkarindji LIP taken from Marshall (2016) and aligned to the palaeogeographic position of Australia at 510 Ma (green outline) as depicted in Lawver et al. (2014).

2. Geochemical data from Emigrant Pass, Carrara Formation: TOC wt % C, $\delta^{13}C_{org}$ (permil), Hg (ppb) and Hg/TOC (ppb/ wt % C). The position of the Olenellus - Eokochaspsis nodosa biozone boundary is from Palmer and Halley (1979) inferred redox conditions are based on framboid size distribution data (Faggetter et al. 2017).
3. Geochemical data from Oak Springs Summit, Pioche Formation: TOC wt % C, $\delta^{13}C_{org}$ (permil), Hg (ppb) and Hg/TOC (ppb/ wt % C). The position of the Olenellus - Eokochaspsis nodosa biozone boundary is from Palmer (1998), inferred redox conditions are based on framboid size distribution data from Faggetter et al. (2017). See Fig. 2 for key.
4. Geochemical data from Ruin Wash, Pioche Formation: TOC wt % C, $\delta^{13}C_{org}$ (permil), Hg (ppb) and Hg/TOC (ppb/ wt % C). The position of the Olenellus - Eokochaspsis nodosa biozone boundary is from Palmer (1998), inferred redox conditions are based on framboid size distribution data from Faggetter et al. (2017). See Fig. 2 for key.
5. Stratigraphic columns showing TOC wt % C through the Carrara and Pioche formations. See Fig. 2 for key.
6. Cross plots of TOC wt % C vs. Hg (ppb) for the Carrara and Pioche formations.
7. Summary of Hg (ppb) and Hg/TOC (ppb/ wt % C) from the Carrara and Pioche formations. The position of the Olenellus - Eokochaspsis nodosa biozone boundary is from Palmer (1998), inferred redox conditions are based on framboid size distribution data from Faggetter et al. (2017). The yellow highlight correlates the Gold Ace Member of the Carrara Formation with the Combined Metals Member of the Pioche, after Palmer (1998). See Fig. 2 for key.

Table 1. Table containing stratigraphic and geochemical data. Rows coloured in grey indicate samples excluded due to low TOC (< 0.01 wt% TOC). Rows coloured in orange indicate the extinction horizon at Oak Springs Summit and Ruin Wash.

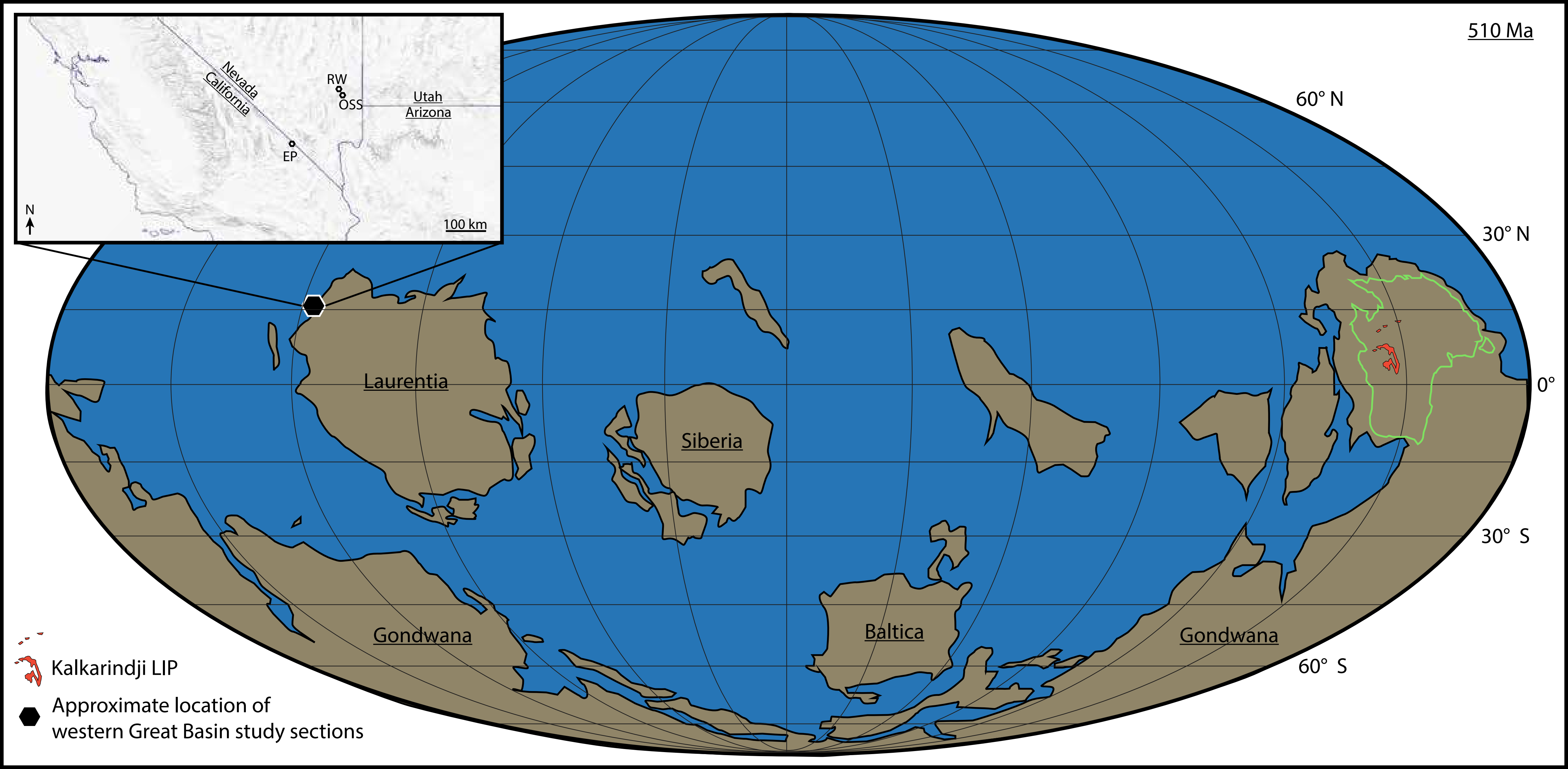
510 Ma
Nevada
California
RW
OSS
Utah
Arizona
EP
N
100 km
60° N
30° N
0°
30° S
60° S
Laurentia
Siberia
Baltica
Gondwana
Gondwana
Kalkarindji LIP
Approximate location of
western Great Basin study sections

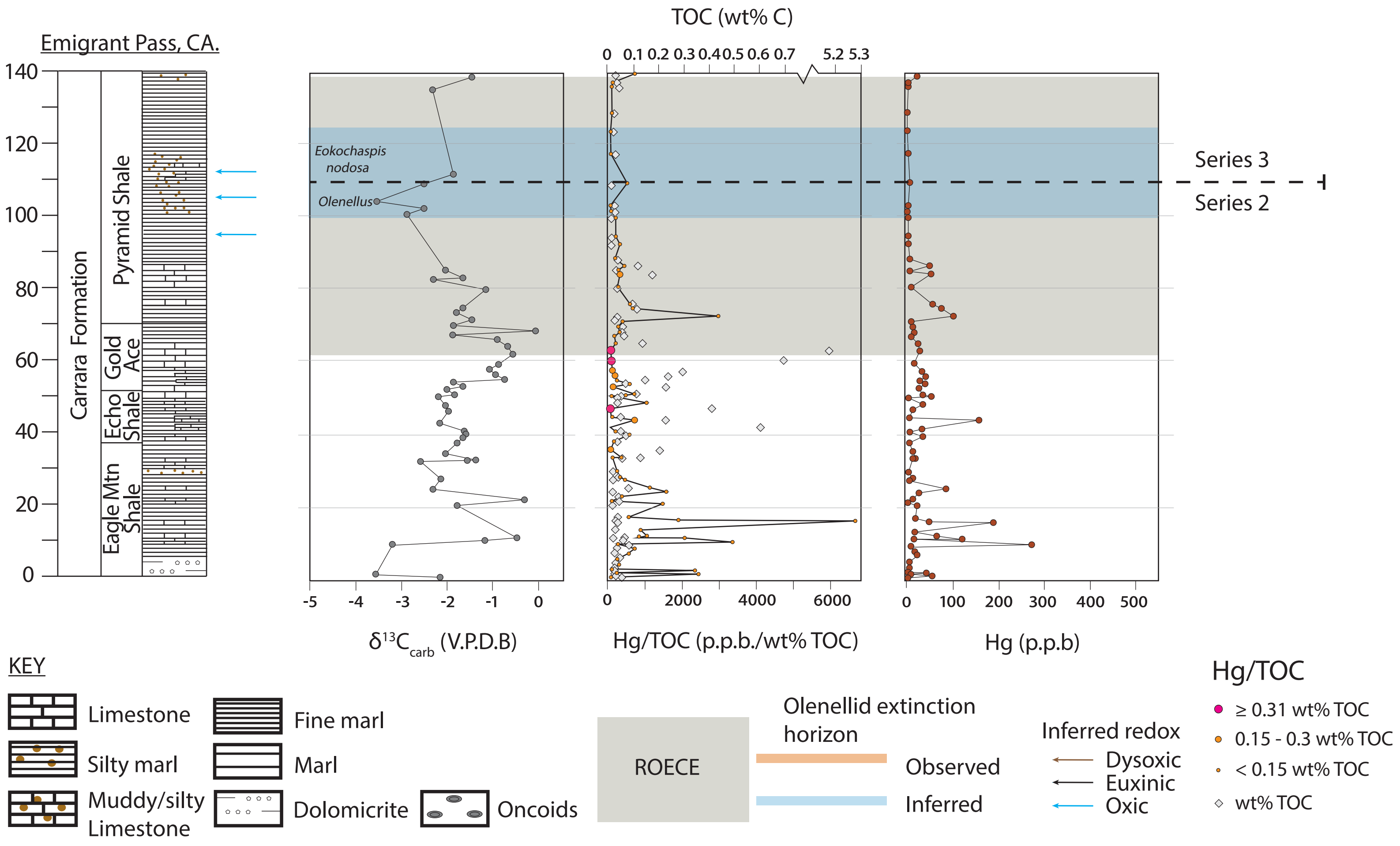

Emigrant Pass, CA.
Carrara Formation
Pyramid Shale
Gold Ace
Echo Shale
Eagle Mtn Shale
Eokochaspis nodosa
Olenellus
Series 3
Series 2
TOC (wt% C)
0 0.1 0.2 0.3 0.4 0.5 0.6 0.7 5.2 5.3
δ13Ccarb (V.P.D.B)
Hg/TOC (p.p.b./wt% TOC)
Hg (p.p.b)
KEY
Limestone
Silty marl
Muddy/silty Limestone
Fine marl
Marl
Dolomicrite
Oncoids
ROECE
Olenellid extinction horizon
Observed
Inferred
Inferred redox
Dysoxic
Euxinic
Oxic
Hg/TOC
≥ 0.31 wt% TOC
0.15 - 0.3 wt% TOC
< 0.15 wt% TOC
wt% TOC

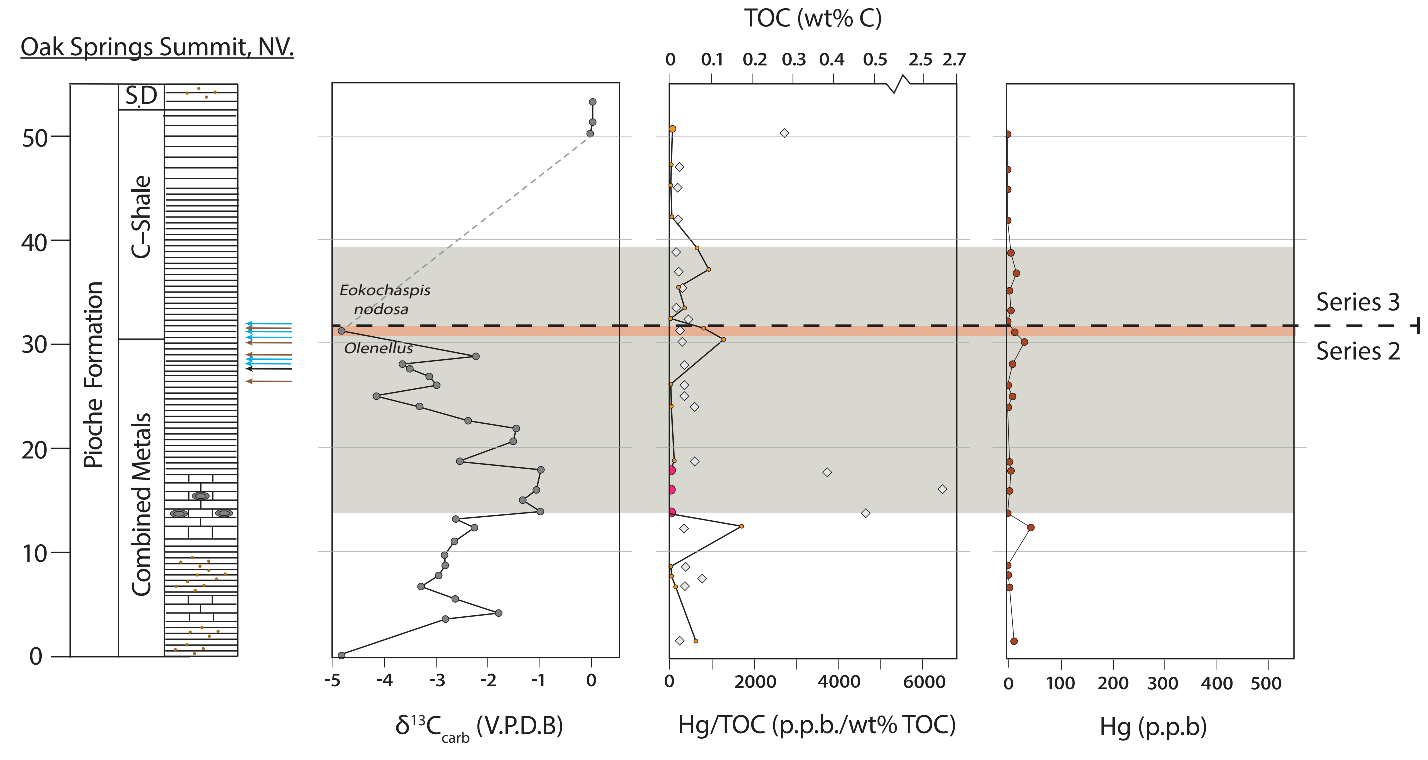

Oak Springs Summit, NV.
TOC (wt% C)
0
0.1
0.2
0.3
0.4
0.5
2.5
2.7
S.D
C–Shale
Pioche Formation
Combined Metals
Eokochaspis nodosa
Olenellus
Series 3
Series 2
0
10
20
30
40
50
-5
-4
-3
-2
-1
0
2000
4000
6000
100
200
300
400
500
δ13Ccarb (V.P.D.B)
Hg/TOC (p.p.b./wt% TOC)
Hg (p.p.b)

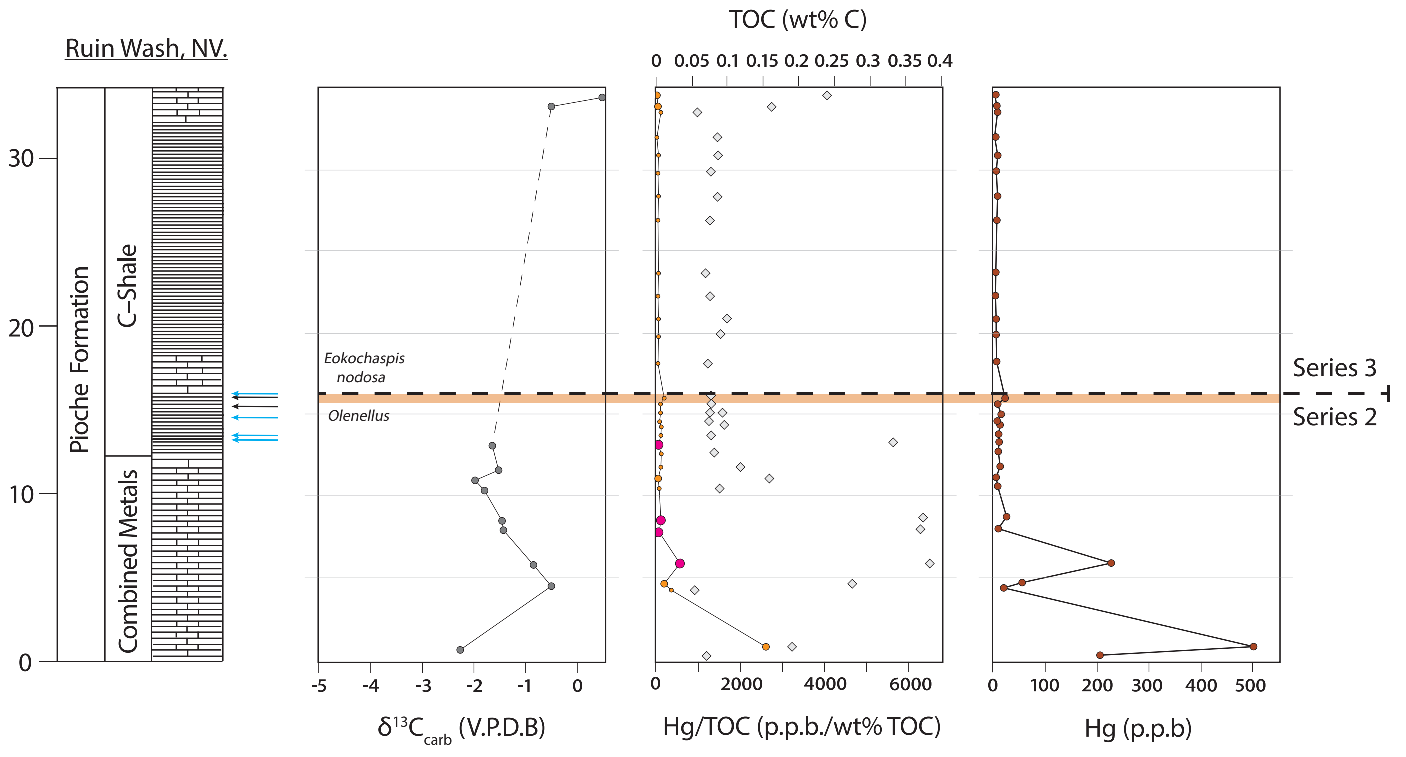

Ruin Wash, NV.
Pioche Formation
C–Shale
Combined Metals
30
20
10
0
Eokochaspis nodosa
Olenellus
Series 3
Series 2
TOC (wt% C)
0 0.05 0.1 0.15 0.2 0.25 0.3 0.35 0.4
-5 -4 -3 -2 -1 0
$\delta^{13}C_{carb}$ (V.P.D.B)
0 2000 4000 6000
Hg/TOC (p.p.b./wt% TOC)
0 100 200 300 400 500
Hg (p.p.b)

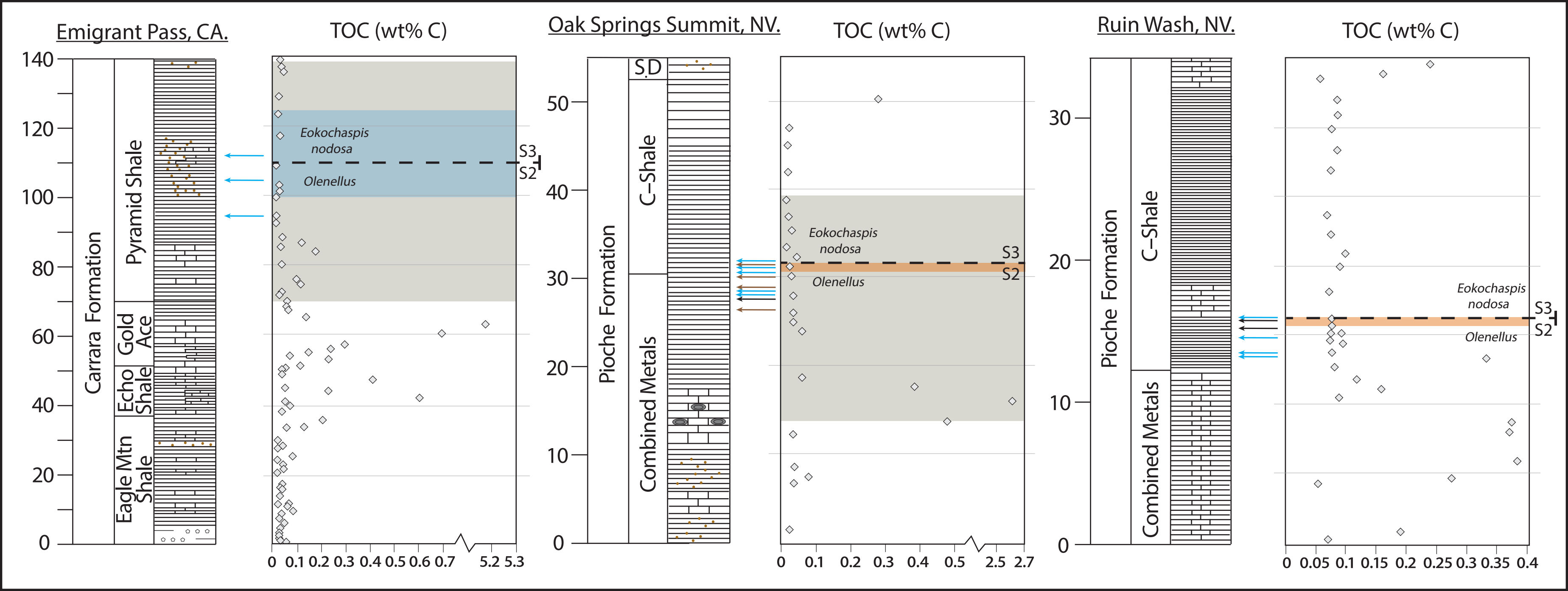

Emigrant Pass, CA.
TOC (wt% C)
Carrara Formation
Pyramid Shale
Gold Ace
Echo Shale
Eagle Mtn Shale
Eokochaspis nodosa
Olenellus
S3
S2
Oak Springs Summit, NV.
TOC (wt% C)
Pioche Formation
S.D
C–Shale
Combined Metals
Eokochaspis nodosa
Olenellus
S3
S2
Ruin Wash, NV.
TOC (wt% C)
Pioche Formation
C–Shale
Combined Metals
Eokochaspis nodosa
Olenellus
S3
S2

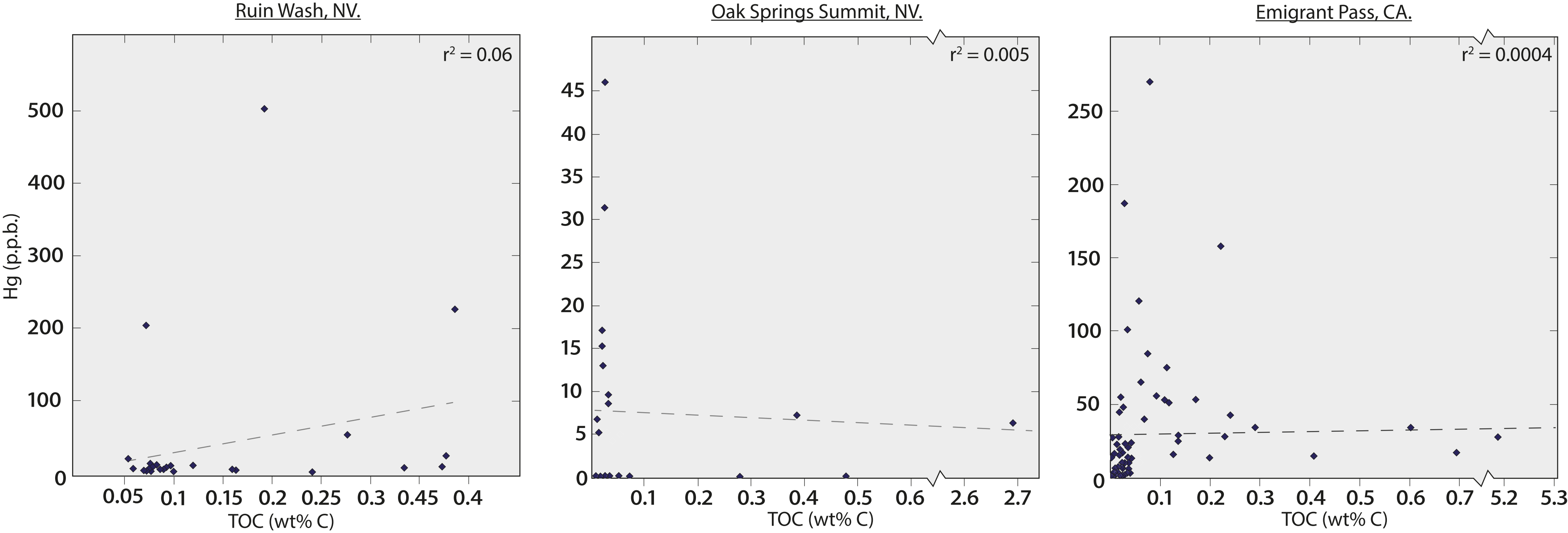

Ruin Wash, NV.
Oak Springs Summit, NV.
Emigrant Pass, CA.
r2 = 0.06
r2 = 0.005
r2 = 0.0004
Hg (p.p.b.)
TOC (wt% C)
TOC (wt% C)
TOC (wt% C)
0
100
200
300
400
500
0.05
0.1
0.15
0.2
0.25
0.3
0.45
0.4
0
5
10
15
20
25
30
35
40
45
0.1
0.2
0.3
0.4
0.5
0.6
2.6
2.7
0
50
100
150
200
250
0.1
0.2
0.3
0.4
0.5
0.6
0.7
5.2
5.3

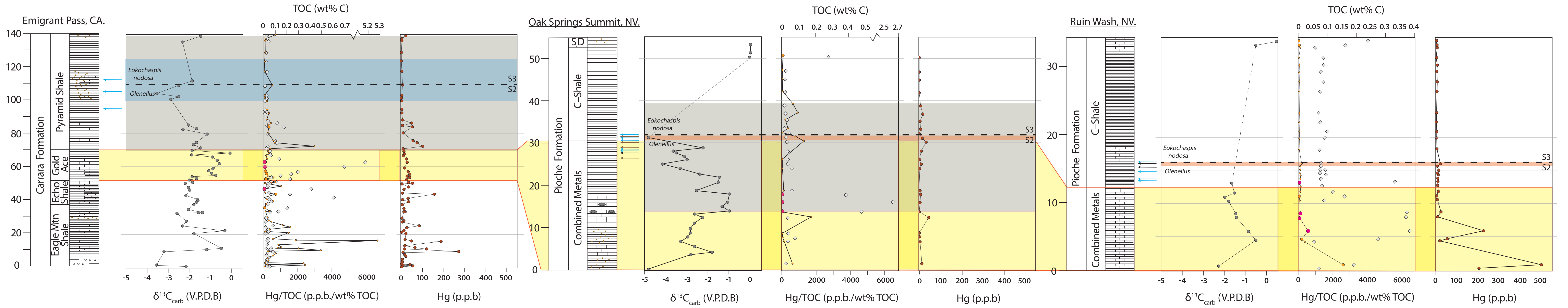

Emigrant Pass, CA.
Carrara Formation
Pyramid Shale
Gold Ace
Echo Shale
Eagle Mtn Shale
Eokochaspis nodosa
Olenellus
TOC (wt% C)
S3
S2
δ13Ccarb (V.P.D.B)
Hg/TOC (p.p.b./wt% TOC)
Hg (p.p.b)
Oak Springs Summit, NV.
Pioche Formation
SD
C-Shale
Combined Metals
Ruin Wash, NV.